2014 22nd International Conference on Pattern Recognition

Piecewise-Bézier C^1 interpolation on Riemannian manifolds with application to 2D shape morphing

Pierre-Yves Gousenbourger
Department of Mathematical Engineering
ICTEAM Institute
Université catholique de Louvain
B-1348 Louvain-la-Neuve, Belgium
pygousenbourger@gmail.com

Chafik Samir
ISIT UMR 6284 CNRS/UdA
Clermont-Ferrand, France
chafik.samir@udamail.fr

P.-A. Absil
Department of Mathematical Engineering
ICTEAM Institute
Université catholique de Louvain
B-1348 Louvain-la-Neuve, Belgium
absil@inma.ucl.ac.be

***Abstract*—We present a new framework to fit a path to a given finite set of data points on a Riemannian manifold. The path takes the form of a continuously-differentiable concatenation of Riemannian Bézier segments. The selection of the control points that define the Bézier segments is partly guided by the differentiability requirement and by a minimal mean squared acceleration objective. We illustrate our approach on specific manifolds: the Euclidean plane (for sanity check), the sphere (as a first nonlinear illustration), the special orthogonal group (with rigid body motion applications), and the shape manifold (with 2D shape morphing applications).**

I. Introduction

The reproduction and use of video sequences of observed objects become increasingly important. As such interest continues to grow, the need for automated methods to analyze shapes of objects also increases. In terms of characterizing objects for detection, classification, and recognition, their shape is naturally an important feature. It already plays an important role in medical diagnostics and surgery guidance, object design, database search, and some forms of disease evolution. Many computer vision applications also use the description of sequences of image to, for instance, reconstruct a missing sequence on the basis of previous and following images. Focusing on these topics, one of our goals in this paper is to develop a new method for modeling the evolution of 2D curves in a smooth and "natural" manner.

In order to leverage the fact that sets of plane curves admit Riemannian manifold structures (see [1] and references therein), we introduce here a new general framework to fit a path to data points on a Riemannian manifold. The problem considered can be broadly formulated as follows: given a sequence of $n+1$ points $(p_0, \ldots, p_n)$ on a Riemannian manifold $\mathcal{M}$ and an increasing sequence of time instants $t_0 < \cdots < t_N$, find a sufficiently regular curve $\gamma : [t_0, t_n] \to \mathcal{M}$ that satisfies $\gamma(t_i) = p_i$, $i = 0, \ldots, n$, where the notion of regularity may involve admissible classes of curves (in particular sufficiently differentiable curves) and optimality criteria. The resulting curve γ can then be viewed as the reconstruction path for the given data. The strategy that drives our approach is to considerably restrict the class of admissible paths (allowing for an algorithm with low space complexity) while keeping it sufficiently large to encompass credible solutions.

A. Related Work

Path fitting on manifolds has been addressed in the literature with different approaches and for various purposes. Generic path fitting methods on manifolds include splines on manifolds [2], rolling procedures [3], subdivision schemes [4], [5], gradient descent [6], and geodesic finite elements [7]. Interpolation of rotations (where the manifold $\mathcal{M}$ is the special orthogonal group $\mathrm{SO}(3)$) is useful in robotics for motion planning of rigid bodies and in computer graphics for the animation of 3D objects [8], [9]. Splines on the sphere have received much attention in the literature; see [10], [11] and references therein. And morphing between shapes can be tackled as an interpolation problem on shape space [12], [13].

We now review a few results that relate more directly to the proposed approach laid out in Sections I-B and II. In Euclidean spaces, Bézier curves are polynomial curves determined by a sequence of control points. The first and last control points are the end points of the curve, but the intermediate control points are in general not on the curve. Bézier curves can be constructed by the classical de Casteljau algorithm [14], which is readily generalized to Riemannian manifolds, replacing line segments by minimal geodesics [15]. The resulting curves are called *generalized Bézier curves* in the work of Popiel and Noakes [16], where formulas for the endpoint velocities and covariant accelerations of these curves are provided. These formulas make it possible to perform C^2 piecewise-Bézier interpolation of a sequence of data points on a Riemannian manifold.

In C^2 interpolation by piecewise cubic Bézier curves, choosing the two intermediate control points of the first segment fully determines all the other control points [16, Example 8]. A difficulty, though, is that the relations between the control points are rather intricate [16, §3], and the idea of choosing the two free intermediate control points in an optimal way (e.g., minimizing the mean squared acceleration) appears intractable.

B. Our Approach

In comparison, by settling for a lower smoothness requirement (C^1 instead of C^2), our method benefits from more freedom, which opens the way for letting a notion of optimality partly guide the choice of the intermediate control points.

1051-4651/14 $31.00 © 2014 IEEE
DOI 10.1109/ICPR.2014.700

Specifically, we seek a C^1 piecewise-Bézier interpolation curve for the data $(p_0, \ldots, p_n)$, such that the segment joining p_0 and p_1, as well as the segment joining p_{n-1} and p_n, are Bézier curves of order two (i.e., with one intermediate control point), while all the other segments are Bézier curves of order three (i.e., with two intermediate control points). In Section II, we point out that, in view of the endpoint velocity formula [16, (6)], fixing the curve velocity vector at each intermediate interpolation point fully determines all the control points, and thus the curve. The task therefore reduces to choosing those velocities. We choose the velocity *directions* in an arbitrary way described in Section II. Then we obtain that, in the Euclidean case, the optimal velocity *magnitudes* minimizing the mean squared acceleration of the curve are solution of a certain tridiagonal linear system of equations. We generalize this linear system to Riemannian manifolds and use it to set the velocity magnitudes at the intermediate interpolation points. Even though the velocity directions are still suboptimal in general and the velocity magnitudes are suboptimal on nonlinear manifolds, the numerical experiments conducted in Section III indicate that the method produces good curves on several manifolds and for a wide range of data point positions, while remaining computationally tractable. The manifolds appearing in the experiments are the two dimensional Euclidean space, the 2-sphere, the rotation group $\mathrm{SO}(3)$, and the shape manifold.

II. C^1 PIECEWISE-BÉZIER INTERPOLATION

In this section, we first describe our approach in $\mathbb{R}^m$, then we present its generalization to manifolds. For simplicity of the exposition, we assume that the time instants are $t_i = i$, but an extension to general time instants is straightforward. Let $t \mapsto \beta_k(t; b_0, \ldots, b_k) = \sum_{i=0}^k b_i B_i^k(t)$ denote the Bézier curve of order k in $\mathbb{R}^m$ with control points $b_0, \ldots, b_k$, where $B_0^k, \ldots, B_k^k$ are the Bernstein basis polynomials of degree k. In this work, we will only make use of Bézier curves of degree 2 and 3, which are given in $\mathbb{R}^m$ by

$$\beta_2(t; b_0, b_1, b_2) = b_0(1-t)^2 + 2b_1 t(1-t) + b_2 t^2 \quad (1)$$

and

$$\begin{aligned}&\beta_3(t; b_0, b_1, b_2, b_3)\\ &\quad = b_0(1-t)^3 + 3b_1 t(1-t)^2 + 3b_2 t^2(1-t) + b_3 t^3. \quad (2)\end{aligned}$$

For more details on Bézier curves in Euclidean spaces, see, e.g., [17]. Referring to Figure 1 for an illustration, we consider the piecewise Bézier curve $\beta : [0, n] \to \mathbb{R}^m$ defined by

$$\beta(t) = \begin{cases} \beta_2(t; p_0, b_1^-, p_1) & \text{if } t \in [0,1] \\ \beta_3(t-(i-1); p_{i-1}, b_{i-1}^+, b_i^-, p_i) & \text{if } t \in [i-1, i], \\ & \quad i = 2, \ldots, n-1 \\ \beta_2(t-(n-1); p_{n-1}, b_{n-1}^+, p_n) & \text{if } t \in [n-1, n], \end{cases} \quad (3)$$

where

$$\begin{aligned} b_i^+ &= p_i + \alpha_i v_i, && i = 1, \ldots, n-2, \\ b_i^- &= p_i - \alpha_i v_i, && i = 2, \ldots, n-1, \\ b_1^- &= p_1 - \tfrac{3}{2}\alpha_1 v_1, \\ b_{n-1}^+ &= p_{n-1} + \tfrac{3}{2}\alpha_{n-1} v_{n-1}. \end{aligned} \quad (4)$$

with $\|v_i\| = 1$ and $\alpha_i \in \mathbb{R}$, $i = 1, \ldots, n-1$. Observe that β satisfies the interpolation conditions $\beta(i) = p_i$, $i = 0, \ldots, n$, and is of class C^1 with $\dot\beta(i) = 3\alpha_i v_i$, $i = 1, \ldots, n-1$ (see, e.g., [16, Theorem 1]).

We choose each v_i arbitrarily as the unitary orientation vector of the bisector of the angle between $p_i - p_{i-1}$ and $p_{i+1} - p_i$, namely, $v_i := \frac{v_i^+ - v_i^-}{\|v_i^+ - v_i^-\|}$ where $v_i^- := (p_{i-1} - p_i)/\|p_{i-1} - p_i\|$ and $v_i^+ := (p_{i+1} - p_i)/\|p_{i+1} - p_i\|$. We then choose the α_i's optimally to minimize the mean squared acceleration of β, i.e.,

$$\begin{aligned}&\int_0^1 \|\ddot\beta_2(t; p_0, b_1^-, p_1)\|^2 \mathrm{d}t \\ &+ \sum_{i=1}^{n-2} \int_0^1 \|\ddot\beta_3(t; p_{i-1}, b_{i-1}^+, b_i^-, p_i)\|^2 \mathrm{d}t \\ &+ \int_0^1 \|\ddot\beta_2(t; p_{n-1}, b_{n-1}^+, p_n)\|^2 \mathrm{d}t\end{aligned}$$

in which the α_i's are involved through (4). Lengthy calculations yield that $\alpha = \begin{bmatrix}\alpha_1 & \ldots & \alpha_n\end{bmatrix}^T$ is the solution of the tridiagonal linear system $\mathbf{A}\alpha = \mathbf{c}$ with

$$\begin{aligned} \mathbf{A}_{(1,1:2)} &= \begin{bmatrix} 12 v_1^T v_1 & 3 v_2^T v_1 \end{bmatrix} \\ \mathbf{A}_{(i,i-1:i+1)} &= \begin{bmatrix} v_{i-1}^T v_i & 4 v_i^T v_i & v_{i+1}^T v_i \end{bmatrix} \\ \mathbf{A}_{(n-1,n-2:n-1)} &= \begin{bmatrix} 3 v_{n-2}^T v_{n-1} & 12 v_{n-1}^T v_{n-1} \end{bmatrix} \end{aligned}$$

and

$$\begin{aligned} \mathbf{c}_{(1)} &= 3 p_2^T v_1 - 2 p_0^T v_1 - p_1^T v_1 \\ \mathbf{c}_{(i)} &= (p_{i+1} - p_{i-1})^T v_i \\ \mathbf{c}_{(n-1)} &= 2 p_n^T v_{n-1} + p_{n-1}^T v_{n-1} - 3 p_{n-2}^T v_{n-1}. \end{aligned}$$

We generalize β to an abstract submanifold $\mathcal{M}$ of a Euclidean space $\mathcal{E}$ as follow. Bézier curves of order k are generalized to $\mathcal{M}$ as in [16, §2]. Equations of the form $b = p + \alpha v$ in (4) are generalized as $b = \mathrm{Exp}_p(\alpha v)$, where Exp denotes the Riemannian exponential (i.e., $t \mapsto \mathrm{Exp}_p(tv)$ is the geodesic on $\mathcal{M}$ with initial position p and velocity v). For $i = 1, \ldots, n-1$, the unit norm vector v_i in the tangent space to $\mathcal{M}$ at p_i is chosen as the unitary orientation vector of the bisector of the angle between $-\mathrm{Log}_{p_i}(p_{i-1})$ and $\mathrm{Log}_{p_i}(p_{i+1})$, where Log denotes the inverse Riemannian exponential. As for the α_i's, they are obtained from the following generalization of the tridiagonal system $\mathbf{A}\alpha = \mathbf{c}$: in matrix $\mathbf{A}$, the inner products $v_i^T v_j$ are replaced by the inner product $\langle v_i, v_j \rangle$ on $\mathcal{E}$, and in $\mathbf{c}$, expressions of the form $(p_j - p_i)^T v_i$ are replaced by $\langle \mathrm{Log}_{p_i} p_j, v_i \rangle$. This yields

$$\begin{aligned} \mathbf{A}_{(1,1:2)} &= \begin{bmatrix} 12\langle v_1, v_1\rangle & 3\langle v_2, v_1\rangle \end{bmatrix} \\ \mathbf{A}_{(i,i-1:i+1)} &= \begin{bmatrix} \langle v_{i-1}, v_i\rangle & 4\langle v_i, v_i\rangle & \langle v_{i+1}, v_i\rangle \end{bmatrix} \\ \mathbf{A}_{(n-1,n-2:n-1)} &= \begin{bmatrix} 3\langle v_{n-2}, v_{n-1}\rangle & 12\langle v_{n-1}, v_{n-1}\rangle \end{bmatrix} \end{aligned}$$

and

$$\begin{aligned} \mathbf{c}_{(1)} &= 3\langle \mathrm{Log}_{p_1}(p_2), v_1\rangle - 2\langle \mathrm{Log}_{p_1}(p_0), v_1\rangle \\ \mathbf{c}_{(i)} &= \langle \mathrm{Log}_{p_i}(p_{i+1}) - \mathrm{Log}_{p_i}(p_{i-1}), v_i\rangle \\ \mathbf{c}_{(n-1)} &= 3\langle \mathrm{Log}_{p_{n-1}}(p_{n-2}), v_{n-1}\rangle - 2\langle \mathrm{Log}_{p_{n-1}}(p_n), v_{n-1}\rangle \end{aligned}$$

There is no guarantee that α remains optimal in this more general setting, but the fact that optimality holds when $\mathcal{M}$ is linear suggests that the results should remain qualitatively adequate on nonlinear manifolds. A confirmation is provided by the experiments presented in Section III.

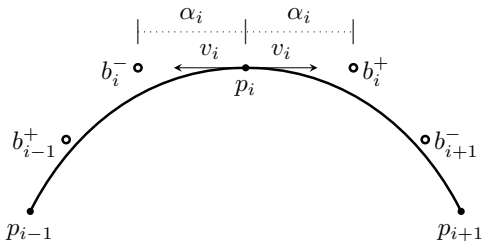

Fig. 1. Illustration of the construction of the piecewise-Bézier curve β in $\mathbb{R}^2$. The path is fully determined by the velocity vectors at the intermediate data points.

III. Results on Specific Manifolds

This section presents results obtained when using our method to generate a C^1 path that interpolates data points on a Riemannian manifold. To help visualize the piecewise-Bézier structure of the generated path, we first illustrate the method on the Euclidean plane $\mathbb{R}^2$ and on the two-dimensional sphere S^2. We then show on SO(3) the reconstruction of the trajectory of a satellite. We finally consider the problem of 2D-object metamorphosis between different time instants, viewed as an interpolation problem on shape space. We show that our method can be used to generate a video animation based on keyframes or to quantify a disease evolution for a medical application when few observations are available.

A. Interpolation on $\mathbb{R}^2$

Figure 2 (first row) is an example of interpolation on the Euclidean plane where the red points are the interpolated data points. The blue curve is the piecewise-Bézier curve generated by the proposed method, and the green points represent the intermediate control points of the Bézier segments. The second row of Figure 2 shows the speed of the curve. We can observe that the resulting curve is C^1 and interpolates the given (red) points as predicted.

Observe that, in this example, the speed is minimal at the intermediate interpolation points. This is due to the particular disposition of the data points which induces a rather sharp turn at those points. The minimal mean squared acceleration criterion thus favors a slower speed around those points.

B. Interpolation on S^2

As second step, we test our method on the unit sphere S^2, which is a nonlinear manifold. The resulting piecewise-Bézier interpolation path is satisfactory for simple configurations of points (figure 3) as for more complicated dispositions (figure 4). In the case of the sphere, the geodesics are great circles and both exponential and log maps between any two points (except antipodal points) have explicit formulas. This makes the algorithm of Section II easy to implement. As

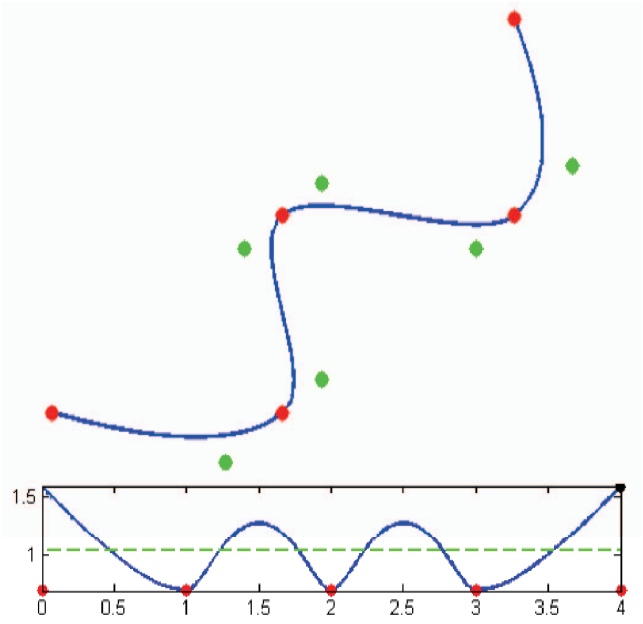

Fig. 2. Interpolation path on $\mathbb{R}^2$. Top: data points (red), intermediate control points (green), and resulting path (blue). Bottom: the speed of the path as a function of t. It is continuous as expected.

on Figure 2, the blue line is the C^1 piecewise-Bézier curve obtained with our approach. It interpolates the four data points (in red) and is driven by the the computed intermediate points (in green).

C. Satellite Trajectory by Interpolation on SO(3)

As an application of the method, we consider the problem of fitting a curve to a finite set of observed rotations of a satellite. The set of 3D rotations is indeed a well known manifold, denoted by SO(3). As for the sphere, the exponential and log maps on SO(3) admit explicit formulas, hence the proposed method is easily applicable. It makes it possible to estimate intermediate rotations on the basis of the observed rotations. We show in Figure 5 that the result is visually very convincing. On the first two rows, we display a sequence of rotations produced by the method at equally spaced time instants. The data points are the initial rotation (first image on the left in the first row), the final rotation (last image of the second row), and three intermediate rotations. The speed of the generated path on SO(3) (lower plot) is continuous as expected.

The method can readily be extended to the special Euclidean group SE(3) of rigid motions by separating the problem into two independent subproblem, one on SO(3) and one on $\mathbb{R}^3$. A extension to SO(3)$\times$S(2) would proceed likewise.

D. Interpolation on Shape Space

As already mentioned, the applicability of the proposed method on a given manifold $\mathcal{M}$ crucially relies on the possibility of computing geodesics between pairs of points on $\mathcal{M}$. This also applies to infinite-dimensional manifolds. As an illustration, we show some convincing results on the

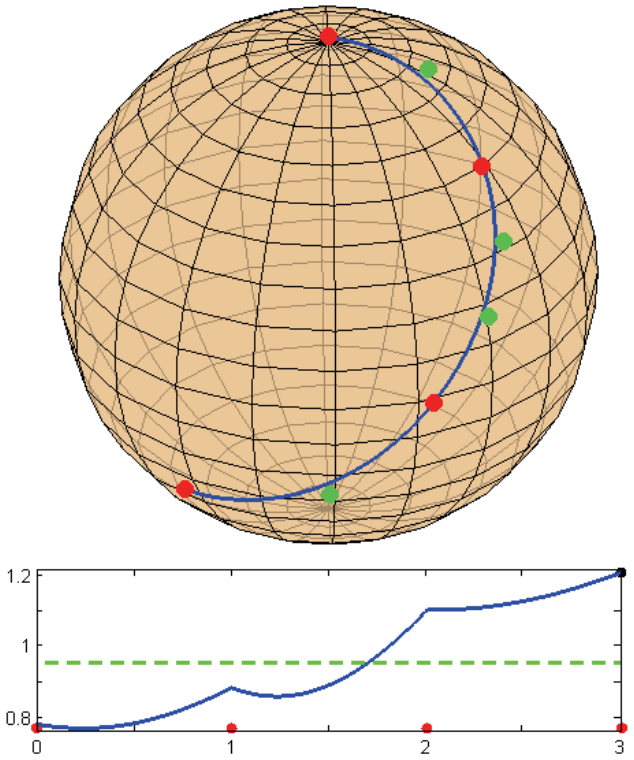

Fig. 3. Example of C^1 curve of interpolation on S^2: the data points (red) are correctly interpolated by the resulting path (blue), which consists of spherical Bézier segments joining the data points and driven by intermediate control points (green).

shape space. By shape in this work, we mean a continuous representation of plane closed curves extracted from images or video sequences. Generally, the plane closed curve represents the boundary of an object.

In our experiments, we represent parametrized curves by their square-root function [18]. This choice, which has been successfully used in many real applications, is motivated by its invariance to translation, rotation, uniform scaling, and re-parametrization [19].

The main steps consist of: (i) defining a space of closed curves of interest, (ii) imposing a Riemannian structure g on it using the elastic metric, and (iii) computing geodesic paths under this metric. Geodesics between two curves represented by their square-root functions q_0 and q_1 are defined to be paths γ on the shape space that are critical points of the energy functional

$$E[\gamma] = \frac{1}{2}\int_0^1 g(\dot{\gamma}(t), \dot{\gamma}(t))\mathrm{d}t \ , \tag{5}$$

under the constraint that $\gamma(0) = q_0$ and $\gamma(1) = q_1$.

We show in Figures 6 and 7 that our approach produces a visually suitable interpolation between given planar shapes. In both cases, the black shapes are the data points and red ones are part of the computed path. The first example is a morphing between a rabbit, a turtle, a bottle and a heart. It is observed that the proposed method yields a path that remains visually adequate in spite of the large deformations between

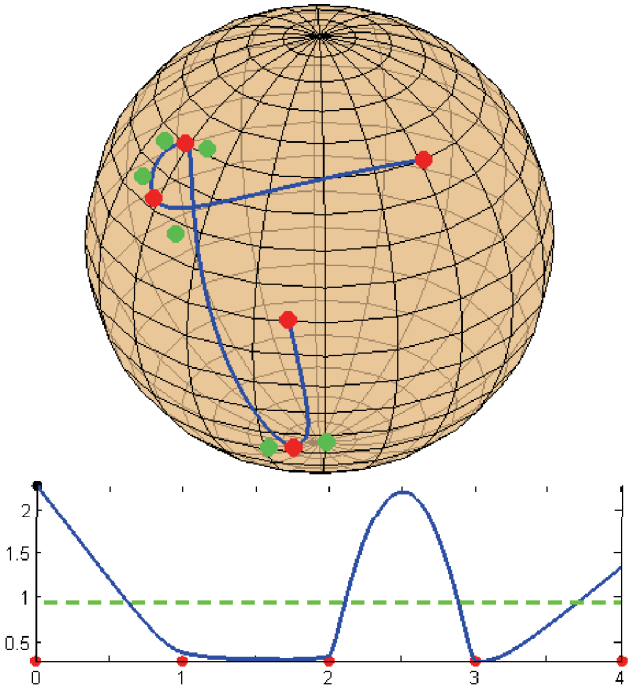

Fig. 4. Example of C^1 curve of interpolation on S^2 with a more complicated dataset: the data points (red) are correctly interpolated by the resulting path (blue), which consists of spherical Bézier segments joining the data points and driven by intermediate control points (green).

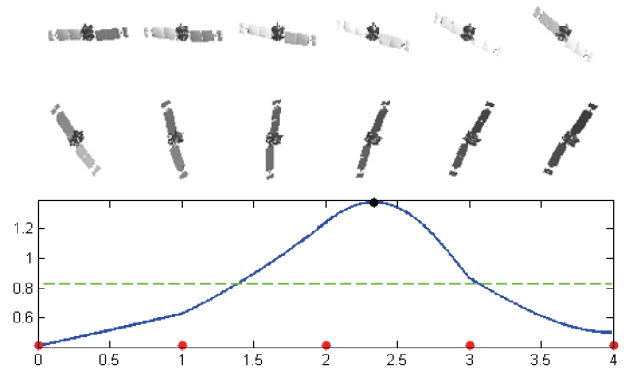

Fig. 5. Top: Smooth C^1 curve of interpolation on $\mathrm{SO}(3)$ for 5 data points. The points on $\mathrm{SO}(3)$ represent rotations of a satellite. Combined with results obtained on S^2, the method readily extends to $\mathrm{SO}(3)\times\mathrm{S}^2$. Bottom: Evolution of the norm of the velocity along the interpolation curve.

the given shapes. The second example is an interpolation between observations of endometrial tissues evolving during different periods of diagnosis.

E. Performances of the Method

The time efficiency of the proposed method on a given manifold $\mathcal{M}$ depends on the availability of fast algorithms to perform the following tasks: (i) compute the Riemannian logarithms and inner products involved in the definition of the v_i's, $\mathbf{A}$, and $\mathbf{c}$; (ii) solve the tridiagonal linear system $\mathbf{A}\alpha = \mathbf{c}$; (iii)

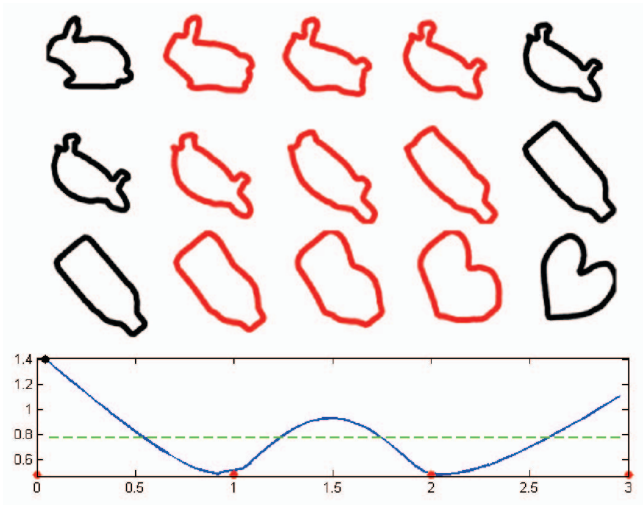

Fig. 6. C^1 path of interpolation on shape spaces. The method still provides a path with continuous velocities. The reconstruction of the deformation path is here illustrated by the morphing between a rabbit, a turtle, a bottle and a heart. The curves are rotated such that the difference between curves is minimized before applying the method. The given shapes are in black while the constructed shapes are in red.

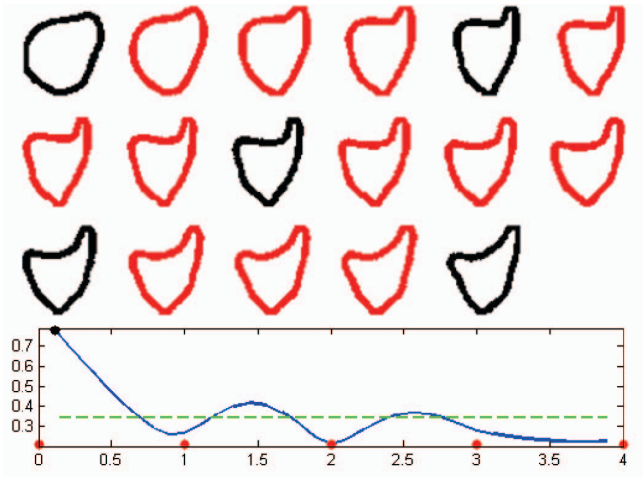

Fig. 7. C^1 path of interpolation on shape spaces applied to a set of observed tissues during a diagnosis.

compute the intermediate control points $b_i^{\pm} = \mathrm{Exp}_{p_i}(\pm\alpha_i v_i)$, $b_1^- = \mathrm{Exp}_{p_1}(-\frac{3}{2}\alpha_1 v_1)$, $b_{n-1}^+ = \mathrm{Exp}_{p_{n-1}}(\frac{3}{2}\alpha_{n-1} v_{n-1})$; (iv) evaluate the piecewise-Bézier curve β at specified time instants using the Riemannian de Casteljau algorithm (see, e.g.,[16, §2]) which itself relies solely on the Riemannian exponential and logarithm. When the number of specified time instants is large, the last task becomes the bottleneck. This is inherent to Bézier curves on manifolds, not to the proposed approach to selecting the piecewise-Bézier curve. As a counterpart, Bézier curves have the advantage of a low space complexity: given the the data points p_i $(i = 0, \ldots, n)$, the piecewise-Bézier curve β generated by the method is fully specified by the velocities $\dot{\beta}(i) = 3\alpha_i v_i$ $(i = 1, \ldots, n-1)$.

IV. Conclusion

We have introduced a new framework to fit a given finite set of data points on Riemannian manifolds. The output of the method is a continuously-differentiable path composed of Riemannian Bézier segments joining the data points. The choice of the intermediate control points that define the Bézier segments is guided in part by minimizing the mean squared acceleration of the piecewize path. The solution of this optimization problem is a tridiagonal linear system depending on known elements of differential geometry permitting the generalization of the formula. To assess the efficiency of the proposed method, we have presented results on specific manifolds: the Euclidean space for illustration, the sphere as a nonlinear space, the special orthogonal group to compute a smooth satellite trajectory, and the shape manifold to characterize shape evolution.

Acknowledgment

This paper presents research results of the Belgian Network DYSCO (Dynamical Systems, Control, and Optimization), funded by the Interuniversity Attraction Poles Programme initiated by the Belgian Science Policy Office. This work was financially supported by the Belgian FRFC (Fonds de la Recherche Fondamentale Collective).

References

[1] W. Mio, A. Srivastava, and S. Joshi, "On shape of plane elastic curves," *Int. J. Comput. Vision*, vol. 73, no. 3, pp. 307 – 324, July 2007.

[2] M. Camarinha, F. Silva Leite, and P. Crouch, "Splines of class C^k on non-Euclidean spaces," *IMA J. Math. Control Inform.*, vol. 12, no. 4, pp. 399–410, 1995.

[3] K. Hüper and F. Silva Leite, "On the geometry of rolling and interpolation curves on S^n, SO_n, and Grassmann manifolds," *J. Dyn. Control Syst.*, vol. 13, no. 4, pp. 467–502, 2007.

[4] J. Wallner, E. Nava Yazdani, and P. Grohs, "Smoothness properties of Lie group subdivision schemes," *Multiscale Model. Simul.*, vol. 6, no. 2, pp. 493–505 (electronic), 2007. [Online]. Available: http://dx.doi.org/10.1137/060668353

[5] N. Dyn, "Linear and nonlinear subdivision schemes in geometric modeling," in *Foundations of computational mathematics, Hong Kong 2008*, ser. London Math. Soc. Lecture Note Ser. Cambridge: Cambridge Univ. Press, 2009, vol. 363, pp. 68–92.

[6] C. Samir, P.-A. Absil, A. Srivastava, and E. Klassen, "A gradient-descent method for curve fitting on Riemannian manifolds," *Found. Comput. Math.*, vol. 12, pp. 49–73, 2012. [Online]. Available: http://dx.doi.org/10.1007/s10208-011-9091-7

[7] O. Sander, "Geodesic finite elements of higher order," Institut für Geometrie und Praktische Mathematik, RWTH Aachen, Tech. Rep. 356, 2013.

[8] Y. Shen, K. Hüper, and F. Silva Leite, "Smooth interpolation of orientation by rolling and wrapping for robot motion planning," in *Robotics and Automation, 2006. ICRA 2006. Proceedings 2006 IEEE International Conference on*, 2006, pp. 113–118.

[9] J. Park, "Interpolation and tracking of rigid body orientations," in *Control Automation and Systems (ICCAS), 2010 International Conference on*, 2010, pp. 668–673.

[10] S. R. Buss and J. P. Fillmore, "Spherical averages and applications to spherical splines and interpolation," *ACM Trans. Graph.*, vol. 20, no. 2, pp. 95–126, Apr. 2001. [Online]. Available: http://doi.acm.org/10.1145/502122.502124

[11] L. Noakes, "Spherical splines," in *Geometric Properties for Incomplete data*, R. Klette, R. Kozera, L. Noakes, and J. Weickert, Eds. Springer Netherlands, 2006, vol. 31, pp. 77–101. [Online]. Available: http://dx.doi.org/10.1007/1-4020-3858-8_5

[12] M. Kilian, N. J. Mitra, and H. Pottmann, "Geometric modeling in shape space," *ACM Trans. Graph.*, vol. 26, no. 3, Jul. 2007. [Online]. Available: http://doi.acm.org/10.1145/1276377.1276457

[13] C. Samir, P. Van Dooren, D. Laurent, K. A. Gallivan, and P.-A. Absil, "Elastic morphing of 2D and 3D objects on a shape manifold," in *Image Analysis and Recognition*, ser. Lecture Notes in Computer Science. Springer-Verlag, 2009, vol. 5627, pp. 563–572.

[14] P. de Casteljau, "Outillages méthodes calcul," 1959, technical Report, André Citroën Automobiles, Paris, 1959.

[15] F. C. Park and B. Ravani, "Bézier curves on Riemannian manifolds and Lie groups with kinematics applications," *J. Mech. Des.*, vol. 117, no. 1, pp. 36–40, 1995.

[16] T. Popiel and L. Noakes, "Bézier curves and C^2 interpolation in Riemannian manifolds," *J. Approx. Theory*, vol. 148, no. 2, pp. 111–127, 2007. [Online]. Available: http://dx.doi.org/10.1016/j.jat.2007.03.002

[17] G. Farin, *Curves and Surfaces for CAGD*, 5th ed. Academic Press, 2002.

[18] S. H. Joshi, E. Klassen, A. Srivastava, and I. Jermyn, "A novel representation for Riemannian analysis of elastic curves in $\mathbf{R^n}$," in *CVPR*, 2007.

[19] C. Samir, A. Srivastava, M. Daoudi, and E. Klassen, "An intrinsic framework for analysis of facial surfaces," *Int. J. Comput. Vision*, vol. 82, no. 1, pp. 80–95, 2009.